Inorganic Chemistry

pubs.acs.org/IC

Article

# $Cu_9O_2(VO_4)_4Cl_2$, the First Copper Oxychloride Vanadate: Mineralogically Inspired Synthesis and Magnetic Behavior

Oleg I. Siidra,* Victoria A. Vladimirova, Alexander A. Tsirlin,* Nikita V. Chukanov, and Valery L. Ugolkov

Cite This: https://dx.doi.org/10.1021/acs.inorgchem.9b02565

Read Online

ACCESS | Metrics & More | Article Recommendations

**ABSTRACT:** A new spin-$^1/_2$ frustrated antiferromagnet, $Cu_9O_2(VO_4)_4Cl_2$, was synthesized via chemical vapor transport method that emulates mineral formation in volcanic fumaroles. $Cu_9O_2(VO_4)_4Cl_2$ is the first copper oxychloride vanadate obtained in the ternary $CuO-V_2O_5-CuCl_2$ anhydrous system. Copper ions constitute a three-dimensional complex framework with a topological structure novel for synthetic compounds but similar to that in the fumarolic mineral yaroshevskite. All of the oxygen atoms except for the O7 site are strongly bonded in the $VO_4$ tetrahedra. The O7 site belongs to an additional oxygen atom ($O_a$) being tetrahedrally coordinated by four Cu atoms, thus forming the $OCu_4$ tetrahedra. The structural formula can be represented as $Cu_3[Cu_6O_2](VO_4)_4Cl_2$ highlighting oxocentered units in the structure. IR spectra reveal several absorption bands at 526, 578, and 601 $cm^{-1}$ interpreted as a characteristic feature of the $OCu_4$ tetrahedra. $Cu_9O_2(VO_4)_4Cl_2$ reveals ferrimagnetic behavior with the Curie temperature $T_C$ = 24 K and the uncompensated moment of $M_r \sim 1.9\ \mu_B$/f.u.

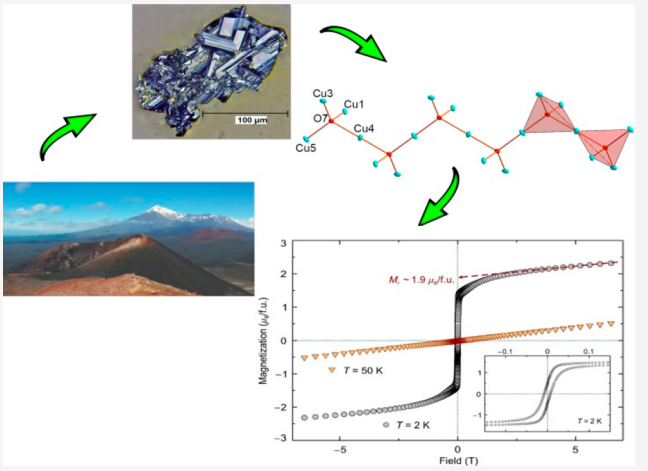




## INTRODUCTION

Copper(II) oxysalt minerals have been of great interest for chemists and physicists, especially in the light of novel magnetic phenomena arising from complex networks of spin-$^1/_2$ $Cu^{2+}$ ions.[1] The disadvantage of minerals is the presence of impurities that hamper or even preclude the study of physical properties on natural samples. However, the discovery of minerals with new structures and chemical compositions facilitates identification of new chemical compounds that can be later prepared in the lab and put under scrutiny of the physical characterization. This approach "from minerals to materials"[2−6] avoids the trial and error method, often used in an exploratory synthesis, and it may be advantageous over computational predictions of thermodynamic stability that can be biased by inaccuracies of the computational methods.

A large number of $Cu^{2+}$ oxysalt minerals are found in nature in the fumaroles with highly oxidizing environments, e.g., on the Tolbachik volcano.[7] Most of these minerals are formed as a result of natural gas transport reactions, i.e., exhalation processes. A typical characteristic of the exhalative copper minerals is the presence of additional oxygen atoms forming oxocentered $OCu_4$ tetrahedra.[8] It is noteworthy that such oxygen atoms are strong Lewis bases. The $OCu_4$ complexes can polymerize via common edges and vertices into structural units of different dimensionality in the structures of exhalative minerals.

The $OCu_4$ tetrahedron also represents the simplest frustrated unit, since it contains four spin triangles with potentially competing magnetic interactions. Many of the copper oxysalt minerals containing the $OCu_4$-based structural fragments demonstrate frustrated antiferromagnetism.[9−11] One of the most impressive examples is averievite $Cu_5O_2(VO_4)\cdot nMClx$ (M = Cu, Cs, Rb, K) discovered more than 20 years ago[12] in the fumaroles of the Tolbachik volcano. Synthetic analogues of this mineral have recently received attention as spin-liquid candidates.[13]

To date, copper oxychloride−vanadates without additional cations have not been reported as synthetic compounds,

Received: August 26, 2019

although a few more complex copper vanadate−chlorides containing alkali[14,15] or/and barium[16,17] metals have been prepared. Herein, we report on the synthesis of $Cu_9O_2(VO_4)_4Cl_2$, the first copper oxychloride vanadate obtained in the ternary $CuO-V_2O_5-CuCl_2$ anhydrous system, and discuss its structural, magnetic, and other properties.

## METHODS

**Synthesis.** By analogy with the mineral yaroshevskite[18] that forms upon high-temperature exhalative processes occurring in the fumarole fields of Tolbachik volcano, crystalline samples of $Cu_9O_2(VO_4)_4Cl_2$ were obtained by the gas-transport reactions from the mixture containing 0.0583 g of CuO (Sigma-Aldrich 99.995%), 0.005 g of $V_2O_5$ (Sigma-Aldrich 99.6%), and 0.0962 g of $CuCl_2$ (Sigma-Aldrich 99%). All of the reagents were predried at 100 °C for 5 h and further rapidly mixed and ground in an agate mortar in air for approximately 5 min. This method resembles crystal growth processes from volcanic gases.[19−22] Precursors were predried at 100 °C for 2 h and further rapidly mixed and ground in an agate mortar in air for 5 min. The reaction mixture was loaded into a quartz ampule (*ca.* 15 × 0.9 cm), which was evacuated ($10^{-2}$ mbar) and further sealed. The ampule was placed horizontally in a tubular furnace Nabertherm and heated up to 600 °C with a rate of 60 °C/h and further held at this temperature for 6 h. The temperature gradient between the source (hot) and deposition (cold) zones of the tube in the furnace was about 50 °C. Then it was slowly cooled with the rate of 5 °C/h down to 550 °C and held for 24 h. Finally, the furnace was slowly cooled to room temperature with the rate of 5.8 °C/h. Well crystalline single-phase aggregates (confirmed by powder X-ray analysis) consisting of black opaque crystals of $Cu_9O_2(VO_4)_4Cl_2$ with a metallic luster (Figure 1)

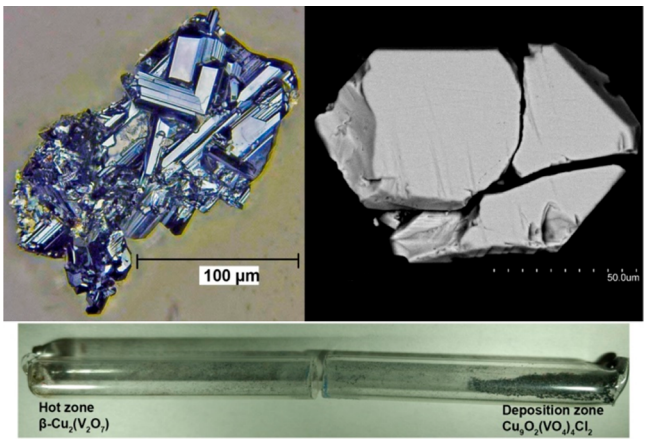


**Figure 1.** Prismatic crystals of $Cu_9O_2(VO_4)_4Cl_2$ (left) and BSE image of the individual crystal (right). Opened ampule with $\beta$-$Cu_2(V_2O_7)$ and $Cu_9O_2(VO_4)_4Cl_2$ (below).

were observed in the deposition zone of the tube, while dark-red crystals of $\beta$-$Cu_2(V_2O_7)$[23] occurred in the source zone. In the course of the gas transport reactions, chloride species transport metals from the source zone to the deposition zone under the action of a temperature gradient. $Cu_9O_2(VO_4)_4Cl_2$ is sensitive to air moisture and light-blue thin films of Cu(OH)Cl[24] start to appear on the crystal faces after 1 week of exposure to air. To prevent decomposition upon hydration, the sample should be kept in an oven at 100 °C or in a glovebox. The yield of the synthesis of $Cu_9O_2(VO_4)_4Cl_2$ is about 41%.

**Chemical Composition.** One crystal (Figure 1) was mounted in epoxy resin and polished with successively decreasing oil suspensions of diamond powders with a finishing size of 0.25 $\mu$m. $Cu_9O_2(VO_4)_4Cl_2$ has been analyzed by energy-dispersive (ED) and wavelength-dispersive (WD) spectrometry. The analyses were obtained using a Hitachi S-3400N scanning electron microscope equipped with an Oxford Instruments X-Max 20 energy dispersive spectrometer (ED, $N$ = 10). The ED spectra were obtained under following conditions: 20 kV accelerating voltage; 1.8 nA beam current; defocused beam (5 $\mu$m spot size); acquisition time 30 s per spectrum. The spectra were processed automatically using the AzTecEnergy software package using the TrueQ technique. Synthetic V metal (V K$\alpha$), Cu metal (Cu K$\alpha$), and KCl (Cl K$\alpha$) were used as standards. $Cu_9O_2(VO_4)_4Cl_2$ is stable under electron beam; no surface damage was observed after analyses. The empirical formula calculated on the basis of 18 anions (16O + 2Cl) per formula unit is $Cu_{9.05}O_2(V_{3.98}O_{16})Cl_2$.

**Single Crystal X-ray Diffraction.** A single crystal of $Cu_9O_2(VO_4)_4Cl_2$ selected for X-ray diffraction (XRD) data collection was mounted on a thin glass fiber and tested on a Bruker APEX II DUO X-ray diffractometer with a Mo−I$\mu$S microfocus X-ray tube ($\lambda$ = 0.71073 Å) operated at 50 kV and 0.6 mA. More than a hemisphere of three-dimensional XRD data was collected with frame widths of 0.5° in $\omega$ and a 20 s count time for each frame. The collected data were integrated and corrected for absorption using a multiscan type model using the Bruker software. Initial atomic coordinates for the crystal structure of $Cu_9O_2(VO_4)_4Cl_2$ were taken from the structure of the previously reported mineral yaroshevskite.[18] The crystal structure was further refined in the $P\bar{1}$ space group to $R_1$ = 0.028 ($wR_2$ = 0.051) for 1705 reflections with $|F_o| \geq 4\sigma F$ by using the SHELXL program.[25] All of the atoms were refined anisotropically. $R_1$ is significantly reduced in the obtained structure refinement of the synthetic material comparing to the structure of the mineral. We may suggest that the disorder of one of Cu sites was not taken into consideration in the refinement of the mineral crystal structure. Although this disorder may also be a characteristic feature of the synthetic material. Main crystallographic information is summarized in Table 1. Selected

**Table 1. Single Crystal and Structure Refinement Data for Synthetic $Cu_9O_2(VO_4)_4Cl_2$**

| crystal data | $Cu_9O_2(VO_4)_4Cl_2$ |
|---|---|
| sp. gr. | $P\bar{1}$ |
| $a$ [Å] | 6.472(4) |
| $b$ [Å] | 8.343(6) |
| $c$ [Å] | 9.206(7) |
| $\alpha$ [deg] | 105.177(12) |
| $\beta$ [deg] | 96.215(11) |
| $\gamma$ [deg] | 107.642(11) |
| $V$ [Å$^3$] | 447.6(5) |
| $Z$ | 1 |
| $\rho_{calc}$ [g·cm$^{-3}$] | 4.209 |
| $\mu$ [mm$^{-1}$] | 12.816 |
| data collection | |
| $\theta$ range [deg] | 2.34−27.99 |
| $hkl$ limits | −8 → +8 |
| | −10 → +11 |
| | −12 → +12 |
| total refln | 5036 |
| unique refln ($R_{int}$) | 2165 (0.0334) |
| unique refln $F > 4\sigma F$ | 1705 |
| refinement | |
| $R_1$ [$F > 4\sigma F$], $wR_2$ [$F > 4\sigma F$] | 0.0282, 0.0508 |
| $R_1$ all, $wR_2$ all | 0.0445, 0.0558 |
| GoF | 0.993 |
| $\Delta\rho_{max}$, $\Delta\rho_{min}$ [e·Å$^{-3}$] | 0.834, −0.648 |

interatomic distances for all atoms are given in Table 2. CCDC-1915553 (CSD, Cambridge) contains the supplementary crystallographic information for synthetic $Cu_9O_2(VO_4)_4Cl_2$.

**Powder X-ray Diffraction.** XRD pattern used for profile matching analysis was recorded in the 2$\theta$ range of 5−100° with a step size of 0.01° using a a Rigaku "MiniFlex II" diffractometer (CoK$\alpha$ radiation, $\lambda$ = 1.7889 Å). The profile matching analysis was carried


https://dx.doi.org/10.1021/acs.inorgchem.9b02565
Inorg. Chem. XXXX, XXX, XXX−XXX

Table 2. Selected Bond Lengths (in Å) in the Structure of $Cu_9O_2(VO_4)_4Cl_2$[k]

| atoms | | atoms | |
|---|---|---|---|
| Cu1–O8 | 1.906(3) | Cu5–O7[a] | 1.922(3) |
| Cu1–O6 | 1.910(3) | Cu5–O7[e] | 1.922(3) |
| Cu1–O5 | 1.954(3) | Cu5–O6[a] | 1.999(3) |
| Cu1–O7 | 1.972(3) | Cu5–O6[e] | 1.999(3) |
| Cu1–O5[a] | 2.571(1) | Cu5–Cl1[d] | 2.937(1) |
| | | Cu5–Cl1[f] | 2.937(1) |
| Cu2–O1 | 1.940(3) | | |
| Cu2–O3[b] | 1.967(3) | Cu6A–O9[g] | 1.875(3) |
| Cu2–O2 | 1.967(3) | Cu6A–O9[h] | 1.875(3) |
| Cu2–O3 | 2.047(3) | Cu6A–O4[a] | 2.048(3) |
| Cu2–Cl1 | 2.566(2) | Cu6A–O4[i] | 2.048(3) |
| Cu3–O7 | 1.915(3) | Cu6B–Cl1[d] | 2.044(13) |
| Cu3–O2 | 1.926(3) | Cu6B–O9[h] | 2.065(14) |
| Cu3–O9[c] | 1.944(3) | Cu6B–O4[i] | 2.142(14) |
| Cu3–O4 | 1.992(3) | | |
| | | V1–O5[a] | 1.669(3) |
| Cu4–O7[d] | 1.916(3) | V1–O4[j] | 1.738(3) |
| Cu4–O7[e] | 1.916(3) | V1–O3[j] | 1.748(3) |
| Cu4–O8[d] | 1.993(3) | V1–O2 | 1.765(3) |
| Cu4–O8[e] | 1.993(3) | | |
| Cu4–Cl1[d] | 2.915(1) | V2–O1 | 1.656(3) |
| Cu4–Cl1[e] | 2.915(1) | V2–O8[d] | 1.717(3) |
| | | V2–O6[a] | 1.730(3) |
| | | V2–O9 | 1.757(3) |

[k]Symmetry transformations used to generate equivalent atoms are shown in footnotes a–j. [a]$-x, -y+1, -z$. [b]$-x+1, -y+1, -z-1$. [c]$x, y+1, z$. [d]$-x+1, -y+1, -z$. [e]$x, y-1, z$. [f]$x-1, y-1, z$. [g]$-x, -y, -z$. [h]$x, y, z+1$. [i]$x, y-1, z+1$. [j]$-x, -y+1, -z-1$.

out in the JANA2006 crystallographic system.[26] The background was fitted using Chebyshev polynomial function, and the peak shapes were described by a pseudo-Voigt_function. The refined unit-cell parameters in the space group $P\bar{1}$ are $a = 6.476(2)$ Å, $b = 8.344(2)$ Å, $c = 9.2071(2)$ Å, $\alpha = 105.172(3)$, $\beta = 96.211(4)°$, $\gamma = 107.648(3)$, and $V = 447(1)$ Å$^3$. The final observed, calculated, and difference powder XRD patterns resulting from the profile matching procedure are plotted in Figure 2.

**Infrared Spectroscopy (FTIR).** In order to obtain infrared (IR) absorption spectrum (Figure 3), powdered sample of $Cu_9O_2(VO_4)_4Cl_2$ was mixed with dried KBr, pelletized, and analyzed using an ALPHA FTIR spectrometer (Bruker Optics) with a resolution of 4 cm$^{-1}$ and 16 scans. The IR spectrum of an analogous pellet of pure KBr was used as a reference.

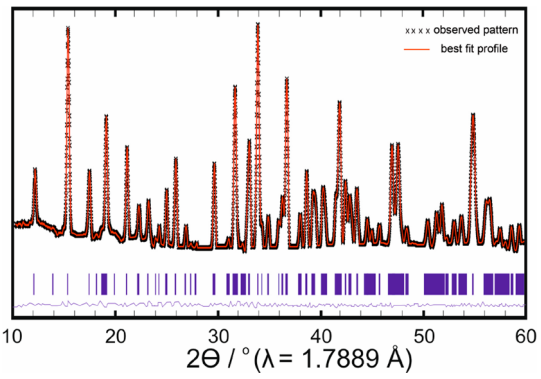


Figure 2. Results of the profile matching analysis of $Cu_9O_2(VO_4)_4Cl_2$ from the powder XRD data.

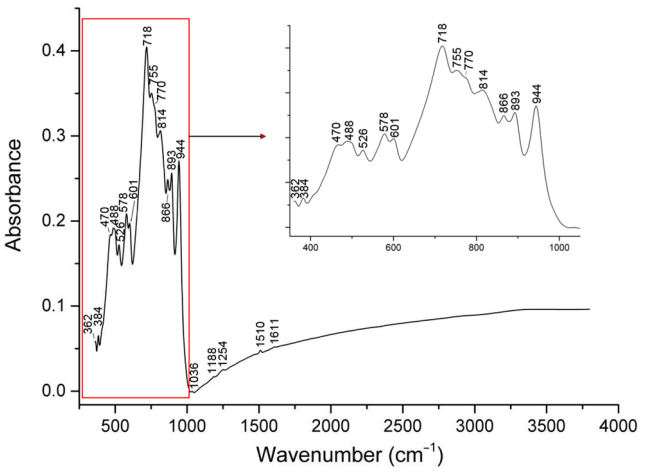


Figure 3. Infrared (FTIR) spectrum of $Cu_9O_2(VO_4)_4Cl_2$.

The IR spectrum of $Cu_9O_2(VO_4)_4Cl_2$ contains two groups of strong bands (in the ranges 450–620 and 700–960 cm$^{-1}$) that correspond to Cu–O and V–O stretching vibrations, respectively. Weak absorptions below 450 cm$^{-1}$ are due to O–V–O bending vibrations.[27] Only very weak peaks corresponding to overtones and combination modes are observed above 1000 cm$^{-1}$.

In the $VO_4$ tetrahedra, V–O bonds are substantially covalent and have relatively high force constants as compared with force characteristics of ionic bonds. For this reason, stretching vibrations of the $VO_4^{3-}$ groups can be considered nearly independent of other lattice vibrations of the crystal. IR bands of V–O stretching vibrations of weakly distorted $VO_4^{3-}$ groups are usually observed in the range 790 to 900 cm$^{-1}$.[27] In the case of $Cu_9O_2(VO_4)_4Cl_2$, a stronger splitting is observed in this spectral region which reflects a significant distortion of the $VO_4$ tetrahedra and the absence of degeneration of V–O stretching modes. This compound has 8 degrees of freedom related to V–O stretching coordinates. Consequently, the number of IR active bands should be 8. This is in a good agreement with the observed spectrum, where 6 absorption maxima, a well-pronounced shoulder at 770 cm$^{-1}$ and a less distinct inflection point at ~830 cm$^{-1}$ are observed in the wavenumber range 700–960 cm$^{-1}$.

Bands of Cu–O stretching lattice modes cannot be assigned to isolated Cu–O bonds. However, contribution of different Cu–O bonds to different normal vibrations can be tentatively supposed based on indirect considerations. In the range 450 to 620 cm$^{-1}$, five absorption maxima are observed. Three of them (at 526, 578, and 601 cm$^{-1}$) are close to the absorption bands at 520, 580, and 612 cm$^{-1}$ in the IR spectrum of the mineral eriaxmanite $Cu_4O(AsO_4)_2$, in which all $Cu^{2+}$ cations are a part of oxocentered tetrahedra. One can suppose that this triplet is a characteristic feature of the $OCu_4$ tetrahedra. Under this assumption, the other two bands (at 470 and 488 cm$^{-1}$) are to be tentatively assigned to Cu–O stretching vibrations predominantly involving O atoms other than O7.

**Thermal Analysis (TG + DSC).** Thermal analysis was performed on a NETZSCH STA 429 CD. Measurements were performed at 40–860 °C. Here, 1.35 mg of the powder sample was used and placed in an alundum crucible with a lid. The heating rate was 10 °C/min. $Cu_9O_2(VO_4)_4Cl_2$ does not demonstrate significant mass loss in the whole temperature range (Figure 4). The maximum observed at 800 °C is due to the melting of the sample.

**Magnetization Measurements.** The magnetic characterization of $Cu_9O_2(VO_4)_4Cl_2$ was performed on a polycrystalline sample using the MPMS SQUID VSM magnetometer from Quantum Design in the temperature range of 1.8–400 K and in magnetic fields up to 7 T.

***Ab Initio* Calculations.** Magnetic exchange couplings in $Cu_9O_2(VO_4)_4Cl_2$ were obtained from density-functional band-structure calculations performed in the FPLO code[28] using generalized gradient approximation (GGA) for the exchange-correlation potential.[29] Individual exchange parameters $J_i$ normalized


https://dx.doi.org/10.1021/acs.inorgchem.9b02565
Inorg. Chem. XXXX, XXX, XXX–XXX

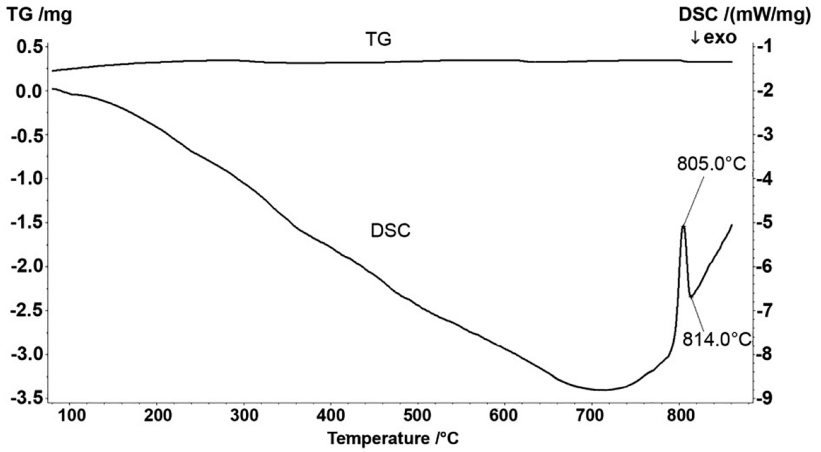


**Figure 4.** TG and DSC curves for $Cu_9O_2(VO_4)_4Cl_2$.

per bond were extracted by a mapping procedure from total energies of four collinear spin configurations, as explained in ref 30. The unit cell doubled along the *a* direction was used. Strong correlation effects in the Cu 3d shell were taken into account on the mean-field level via GGA+*U* with the on-site Coulomb repulsion parameter $U_d$ = 9.5 eV and Hund's coupling $J_d$ = 1 eV.[31,32]

## RESULTS AND DISCUSSION

**Structure Analysis.** The crystal structure of $Cu_9O_2(VO_4)_4Cl_2$ contains six symmetrically independent Cu sites (Figure 5) with different coordination environments. All

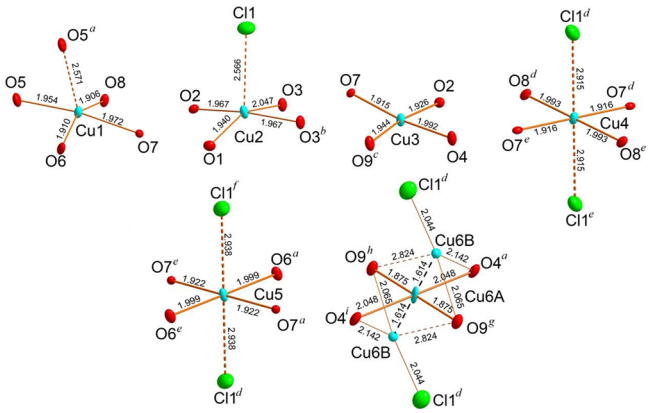

**Figure 5.** Coordination environments of $Cu^{2+}$ cations in the structure of $Cu_9O_2(VO_4)_4Cl_2$ (Note: Cu6A site S.O.F. = 92%; Cu6B site S.O.F. = 8%). Cu−O and Cu−Cl bonds >2.5 Å are shown by orange dotted lines. Symmetry transformations used to generate equivalent atoms: (a) $-x, -y + 1, -z$; (b) $-x + 1, -y + 1, -z - 1$; (c) $x, y + 1, z$; (d) $-x + 1, -y + 1, -z$; (e) $x, y - 1, z$; (f) $x - 1, y - 1, z$; (g) $-x, -y, -z$. (h) $x, y, z + 1$; (i) $x, y - 1, z + 1$; (j) $-x, -y + 1, -z - 1$; (k) $-x + 2, -y, -z - 1$; (l) $x + 1, y - 1, z$; (m) $x + 1, y, z - 1$; (n) $x - 1, y + 1, z$; (o) $-x, -y + 2, -z$; (p) $-x + 1, -y + 2, -z$.

of the copper sites have four Cu−O bonds ≤2.05 Å, thus forming $CuO_4$ squares with different degree of distortion. The refinement showed that the Cu6 site is split over Cu6A and Cu6B with s.o.f. = 92% and s.o.f. = 8%, respectively. Addison tau-parameter has been used to describe the distortion around Cu1 and Cu2 sites. Values of $\tau$ = 0.20 and $\tau$ = 0.35 for Cu1 and Cu2 sites, respectively, were calculated. The $Cu1O_4$ square is complemented by the long Cu1−O5 bond of 2.571(1) Å, thus forming a distorted tetragonal pyramid. In a similar manner, the $Cu2O_4$ square is also complemented by the fifth Cu1−Cl1 bond of 2.566(2) Å. Cu4 and Cu5 sites coordination environments are complemented by two apical $Cl^-$ anions each. As a result, an elongated $[CuO_4Cl_2]$ octahedron is formed for both of these sites. The $[CuO_4Cl_2]$ octahedra are distorted owing to the Jahn−Teller effect.[33] The coordination environment of Cu6A site is a regular square, whereas the coordination of the very sparsely occupied 6B site is much more irregular.

Two symmetrically independent tetrahedral V sites are occupied by $V^{5+}$. V−O bond lengths and angles fall within the range typically observed in vanadate structures. All of the oxygen atoms except for O7 are each strongly bonded in the $VO_4$ tetrahedra. The O7 site belongs to an additional oxygen atom[8] ($O_a$) being tetrahedrally coordinated by four Cu atoms each (Figure 6). The O7 atom is tetrahedrally coordinated by Cu1, Cu3, Cu4 and Cu5 atoms, thus forming an $O7Cu_4$ oxocentered tetrahedron. The average ⟨O7−Cu⟩ bond length in $Cu_9O_2(VO_4)_4Cl_2$ is 1.931 Å.

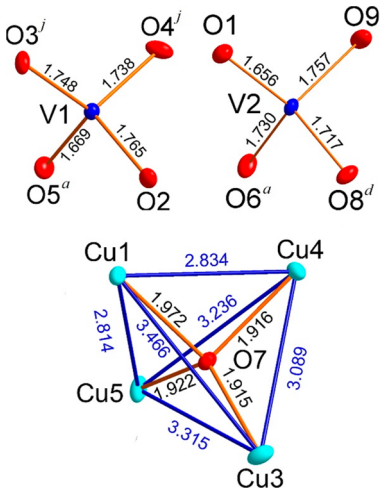

**Figure 6.** Two symmetrically independent $VO_4$ tetrahedra in the structure of $Cu_9O_2(VO_4)_4Cl_2$(top). The coordination of the additional O7 atom and the Cu−Cu distances (blue) in the $Cu_4$ tetrahedron (bottom). Displacement ellipsoids are drawn at 80% probability level. Symmetry transformations used to generate equivalent atoms are given in the Figure 5 caption.


https://dx.doi.org/10.1021/acs.inorgchem.9b02565
Inorg. Chem. XXXX, XXX, XXX−XXX

In the $Cu_9O_2(VO_4)_4Cl_2$ structure, the $OCu_4$ tetrahedra share common corners, thus forming $[O_2Cu_6]^{8+}$ single chains shown in Figure 7. Each of the $OCu_4$ tetrahedra is bidentate.

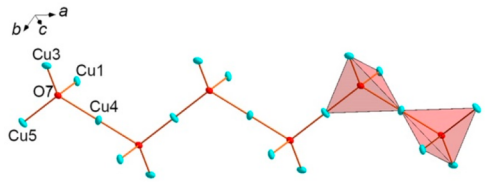


**Figure 7.** General projection of the $[Cu_6O_2]^{8+}$ cationic chain in the $Cu_9O_2(VO_4)_4Cl_2$ structure. Displacement ellipsoids are drawn at 80% probability level.

The topology of the $[O_2Cu_6]^{8+}$ chain in $Cu_9O_2(VO_4)_4Cl_2$ is very similar to the $[Si_2O_6]^{4-}$ silicate chain in the minerals of the pyroxene group,[34] where each $SiO_4$ tetrahedron is replaced by an oxocentered $OCu_4$ tetrahedron. The $[O_2Cu_6]^{8+}$ chains in $Cu_9O_2(VO_4)_4Cl_2$ are known in $Cu^{2+}$ oxysalts[20,35] and can be described as fragments of kagome-nets.[36] Note that Cu2 and Cu6 do not form Cu−$O_a$ bonds with additional oxygen atoms, and thus are not parts of the oxocentered tetrahedra. The structural formula of $Cu_9O_2(VO_4)_4Cl_2$ can be then written as $Cu_3[Cu_6O_2](VO_4)_4Cl_2$ highlighting the oxocentered units in the structure.

All of the Cu-centered polyhedra form complex copper oxide framework in $Cu_9O_2(VO_4)_4Cl_2$ (Figure 8, 9) with voids filled by the $VO_4^{3-}$ and $Cl^-$ anions. Copper oxide framework (Figure 9a) can be split into chains (Figure 9b) formed by Cu2-, Cu3- and Cu6-centered squares and layers (Figure 9c) formed by Cu1-, Cu4- and Cu5-centered polyhedra.

**Magnetism.** Above 200 K, $Cu_9O_2(VO_4)_4Cl_2$ shows paramagnetic behavior with the linear temperature dependence of the inverse susceptibility (Figure 10). The fit with the Curie−Weiss law $\chi = C/(T - \theta)$ returns the antiferromagnetic Curie−Weiss temperature $\theta = -95$ K and Curie constant $C = 3.55$ emu K/mol that corresponds to the paramagnetic effective moment of $\mu = 1.78\ \mu_B$/Cu in good agreement with 1.73 $\mu_B$ expected for an individual spin-$^1/_2$ $Cu^{2+}$ ion and confirms that above 200 K all $Cu^{2+}$ spins fluctuate randomly.

Below 50 K, the susceptibility becomes field-dependent (Figure 10). In lower fields, it shows an abrupt increase that signals the development of an uncompensated magnetic moment and coincides with the hysteretic behavior of the field-dependent magnetization measured at 2 K (Figure 11). This behavior should be contrasted with the linear magnetization curve at 50 K. From the peak in Fisher's heat capacity $d(\chi T)/dT$ we estimate the transition temperature of $T_C = 24$ K (Figure 10). The linear regime of the low-temperature $M(H)$ curve between 4 and 7 T can be extrapolated to zero field yielding the uncompensated moment of $M_r \sim 1.9\ \mu_B$/f.u. Only a narrow hysteresis associated with this uncompensated moment can be seen in the data. The coercive field is 7 mT at 2 K.

The finite value of $M_r$ can be caused by a spin canting in an otherwise antiferromagnetic state or by several ferromagnetic sublattices that are antiferromagnetically coupled but carry different magnetic moments and do not compensate each other. With six nonequivalent Cu sites, the $Cu_9O_2(VO_4)_4Cl_2$ structure contains dozens of possible exchange pathways, yet our microscopic analysis shows that only eight of them give rise to strong magnetic couplings with absolute values in excess of 50 K (Table 3). The first six couplings ($J_1$−$J_6$) are nonfrustrated and form layers in the *ac* plane (Figure 12a).

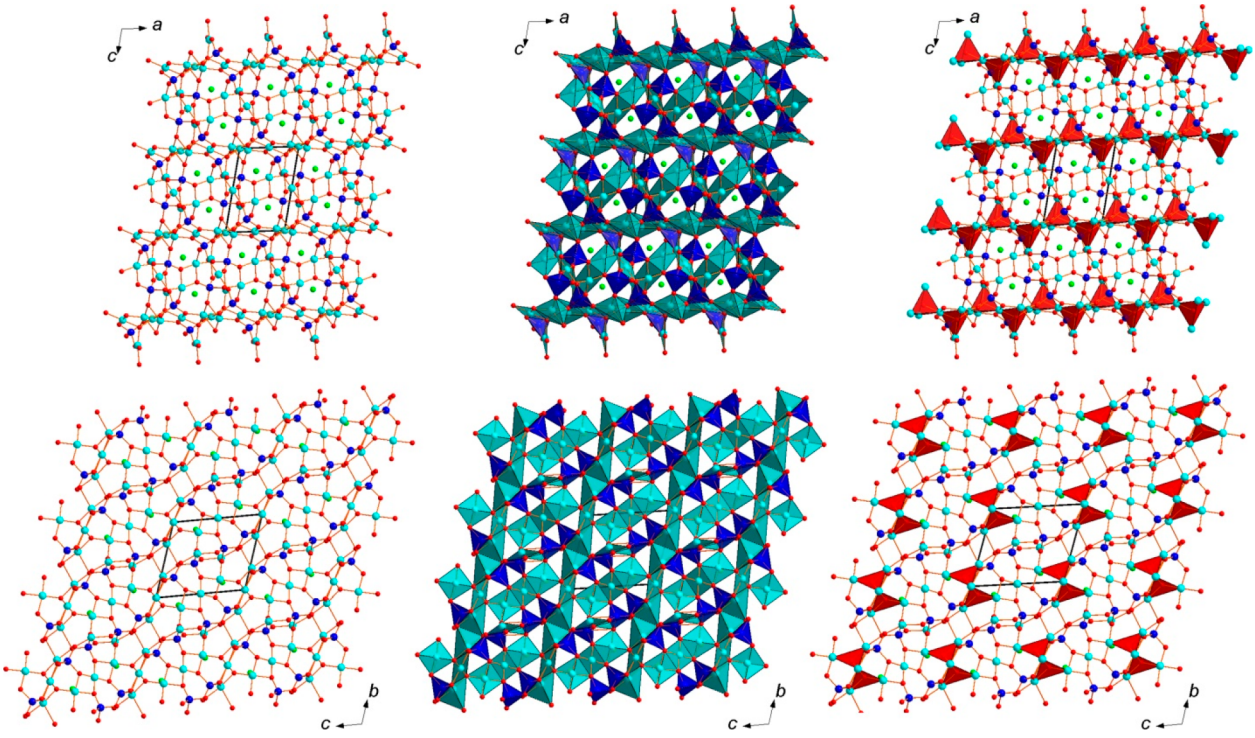


**Figure 8.** General projections of the crystal structure of $Cu_9O_2(VO_4)_4Cl_2$ along the *b* and *a* axes. The Cu−Cl bonds are not shown for clarity. The Cu6 sites are represented as fully ordered. $VO_4$ tetrahedra = blue; $CuO_n$ polyhedra = sky blue; $OCu_4$ tetrahedral units = red.


https://dx.doi.org/10.1021/acs.inorgchem.9b02565
Inorg. Chem. XXXX, XXX, XXX−XXX

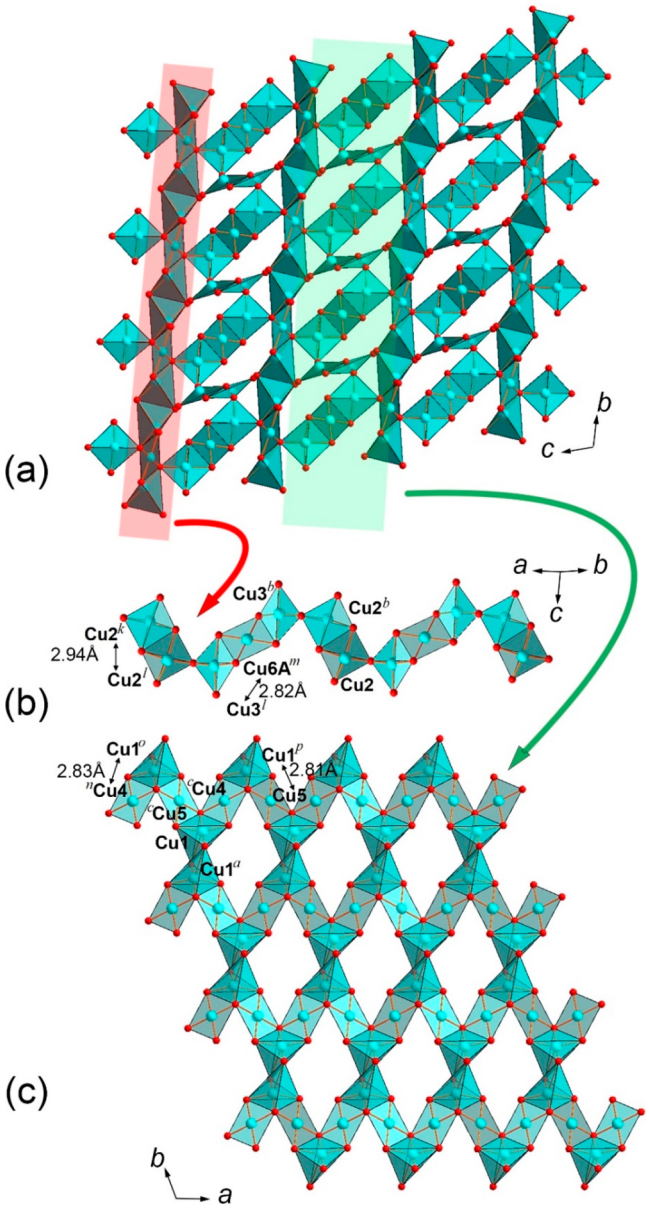


**Figure 9.** Copper-oxide framework (a) in $Cu_9O_2(VO_4)_4Cl_2$. The framework can be split into chains (b) formed by Cu2-,Cu3- and Cu6A-centered squares and complex layers (c) formed by Cu1-, Cu4- and Cu5-centered squares and distorted tetragonal pyramids. The low-occupied Cu6B sites are not shown for clarity. Symmetry transformations used to generate equivalent atoms are given in Figure 5 caption.

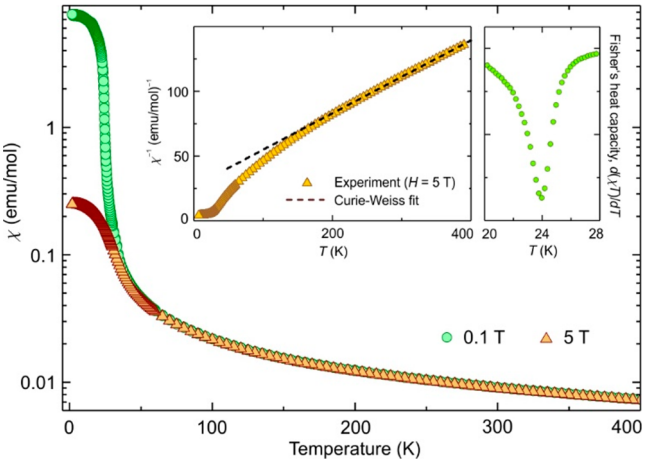


**Figure 10.** Temperature-dependent magnetic susceptibility of $Cu_9O_2(VO_4)_4Cl_2$ measured in the applied fields of 0.1 and 5 T. The insets show the Curie–Weiss fit of the 5 T data and Fisher's heat capacity $d(\chi T)/dT$ calculated based on the 0.1 T data.

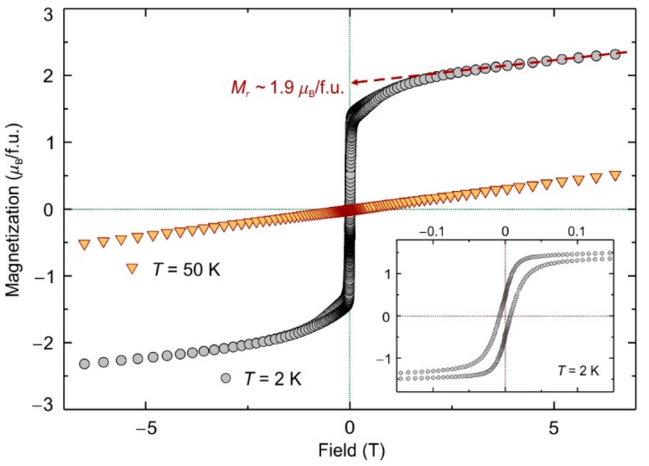


**Figure 11.** Field-dependent magnetization of $Cu_9O_2(VO_4)_4Cl_2$ measured at 2 and 50 K. The dashed line is the extrapolation to zero field that yields the uncompensated moment $M_r \sim 1.9\ \mu_B$/f.u. The inset shows the magnified view of the narrow hysteresis observed at 2 K.

**Table 3. Magnetic Exchange Couplings in $Cu_9O_2(VO_4)_4Cl_2$ Obtained by the GGA+U Mapping Procedure**[a]

| | Cu atoms | $d_{Cu-Cu}$ (Å) | $J_i$ (K) |
|---|---|---|---|
| $J_1$ | Cu1–Cu4 | 2.814 | −78 |
| $J_2$ | Cu3–Cu6 | 2.821 | −90 |
| $J_3$ | Cu1–Cu5 | 2.834 | −83 |
| $J_4$ | Cu2–Cu3 | 3.230 | 140 |
| $J_5$ | Cu3–Cu4 | 3.315 | 175 |
| $J_6$ | Cu1–Cu3 | 3.465 | 255 |
| $J_7$ | Cu1–Cu1 | 5.629 | 65 |
| $J_8$ | Cu1–Cu1 | 5.668 | 60 |

[a]Only the couplings with absolute values in excess of 50 K are listed.

These six couplings would produce collinear ferrimagnetic order with opposite spin directions on the Cu1, Cu2, Cu4, and Cu5 sites on one hand and the Cu3 and Cu6 sites on the other. The resulting net magnetization of $M_r/M_s = {}^1/_3$ exceeds the experimental value of $M_r/M_s \sim 0.21$ by about 50%. However, anisotropic nature of the system may require fields above 7 T in order to reach full net magnetization for some of the field directions.[37] This will reduce the $M_r$ value measured on a polycrystalline sample.

Another possible explanation for our experimental $M_r$ value is spin canting. Indeed, antiferromagnetic couplings $J_7$ and $J_8$ are incompatible with the ferrimagnetic order driven by the other six couplings. This frustration scenario resembles the mineral francisite and its synthetic analogs, $Cu_3Bi(SeO_3)O_2X$ (X = Cl, Br).[37,38] Their magnetic model entails competing nearest-neighbor ferromagnetic ($J_1^{(F)}$) and second-neighbor antiferromagnetic ($J_2^{(F)}$) couplings, with the superscript F standing for "francisite". Whereas $J_1^{(F)}$ would stabilize ferromagnetic order within the Cu planes, the couplings $J_2^{(F)}$


https://dx.doi.org/10.1021/acs.inorgchem.9b02565
Inorg. Chem. XXXX, XXX, XXX–XXX

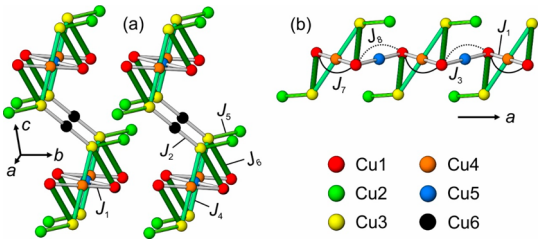


**Figure 12.** Spin−lattice of $Cu_9O_2(VO_4)_4Cl_2$ obtained from *ab initio* calculations. White lines denote ferromagnetic couplings $J_1$−$J_3$, and green lines show nearest-neighbor antiferromagnetic couplings $J_4$−$J_6$, whereas solid and dotted black lines stand for the second-neighbor antiferromagnetic couplings $J_7$ and $J_8$. (a) Magnetic layers in the *ac* plane. Here, $J_7$ and $J_8$ are not shown, and the spin−lattice is nonfrustrated, because triangular loops are formed by one ferromagnetic ($J_1$) and two antiferromagnetic ($J_4$, $J_6$) couplings. Such a spin−lattice is expected to develop collinear ferrimagnetic order with $M_r/M_s = {}^1/_3$. (b) Magnetic ribbon running along the *c* direction highlights the competition between $J_1$, $J_3$ and $J_7$, $J_8$. Note the similarity to $Cu_3Bi(SeO_3)_2O_2Cl$, where every second atom features an antiferromagnetic second-neighbor coupling.[39]

oppose parallel spin alignment and lead to a canted magnetic order,[39] which is well documented experimentally.[37,38] The size of the net moment within each Cu plane is then controlled by the ratio between $J_1^{(F)}$ and $J_2^{(F)}$ and may not be a simple fraction of $M_s$. A similar canting scenario can be envisaged in our case, where $J_1$ and $J_3$ act as $J_1^{(F)}$ and would cause parallel spin alignment of Cu1, Cu4, and Cu5 along the ribbon shown in Figure 12b, whereas $J_7$ and $J_8$ act as $J_2^{(F)}$ and oppose this order.

Distinguishing between these scenarios, ferrimagnetic order with strongly anisotropic magnetization vs spin canting, requires dedicated work on single crystals of $Cu_9O_2(VO_4)_4Cl_2$ and goes beyond the scope of our present study. Nevertheless, already with the data at hand we can conclude that magnetic order in $Cu_9O_2(VO_4)_4Cl_2$ is impeded, with the ratio $|\theta|/T_C \sim 4$ indicating sizable frustration and/or a low-dimensional nature of the spin system. Our microscopic analysis supports magnetic low-dimensionality, because the couplings in the *ac* plane are much stronger than those along the *b* direction (Figure 12a). We also identify the competition between nearest-neighbor ferromagnetic and second-neighbor antiferromagnetic couplings as the plausible mechanism of frustration in this compound.

## CONCLUSION

The novel compound $Cu_9O_2(VO_4)_4Cl_2$ was synthesized via a chemical vapor transport reaction in evacuated silica tubes that emulates natural mineral formation through fumarolic processes. The three-dimensional complex copper oxide substructure is made up of $CuO_4$ squares, for some of them complemented by the additional longer Cu−O bonds. The $OCu_4$ tetrahedral units are polymerized into $[O_2Cu_6]^{8+}$ cationic chains. The refinement of the triclinic crystal structure of $Cu_9O_2(VO_4)_4Cl_2$ showed the presence of disorder for one of the Cu sites. Such a disorder was not previously reported in the structure of the natural sample.

$Cu_9O_2(VO_4)_4Cl_2$ undergoes a magnetic transition at 24 K and develops a sizable net magnetization $M_r/M_s \sim 0.21$. The $|\theta|/T_C \sim 4$ ratio shows that magnetic order sets in at a temperature much lower than the energy scale of magnetic couplings. This indicates that low-dimensionality and frustration, both pinpointed by our microscopic analysis, should be important ingredients of the $Cu_9O_2(VO_4)_4Cl_2$ physics.

## ASSOCIATED CONTENT

### Accession Codes

CCDC 1915553 contains the supplementary crystallographic data for this paper. These data can be obtained free of charge via www.ccdc.cam.ac.uk/data_request/cif, or by emailing data_request@ccdc.cam.ac.uk, or by contacting The Cambridge Crystallographic Data Centre, 12 Union Road, Cambridge CB2 1EZ, UK; fax: +44 1223 336033.

## AUTHOR INFORMATION

### Corresponding Authors

**Oleg I. Siidra** − *Department of Crystallography, St. Petersburg State University, 199034 St. Petersburg, Russia; Kola Science Center, Russian Academy of Sciences, Apatity 184200, Russia;* orcid.org/0000-0003-1908-3152; Email: o.siidra@spbu.ru

**Alexander A. Tsirlin** − *Experimental Physics VI, Center for Electronic Correlations and Magnetism, Institute of Physics, University of Augsburg, 86135 Augsburg, Germany;* Email: altsirlin@gmail.com

### Authors

**Victoria A. Vladimirova** − *Department of Crystallography, St. Petersburg State University, 199034 St. Petersburg, Russia*

**Nikita V. Chukanov** − *Institute of Problems of Chemical Physics, , Chernogolovka 142432, Russia*

**Valery L. Ugolkov** − *Grebenshchikov Institute of Silicate Chemistry, Russian Academy of Sciences, 199034 St. Petersburg, Russia*

Complete contact information is available at: https://pubs.acs.org/10.1021/acs.inorgchem.9b02565

### Notes

The authors declare no competing financial interest.

## ACKNOWLEDGMENTS

This work was financially supported by the Russian Foundation for Basic Research, Grant No. 19-05-00413. Technical support by the SPbSU Resource Centres is gratefully acknowledged. A.A.T. was supported by the Federal Ministry for Education and Research through the Sofja Kovalevskaya Award of the Alexander von Humboldt Foundation. IR spectroscopy studies (N.V.C.) were performed as a part of State Task No. 0089-2019-0013.

## REFERENCES

(1) Inosov, D. S. Quantum Magnetism in Minerals. *Adv. Phys.* **2018**, *67*, 149−252.

(2) Chapman, D. M.; Roe, A. L. Synthesis, Characterization and Crystal Chemistry of Microporous Titanium-Silicate Materials. *Zeolites* **1990**, *10*, 730−737.

(3) Depmeier, W. Minerals as Advanced Materials. *Cryst. Res. Technol.* **2009**, *44*, 1122−1130.

(4) McMillen, C. D.; Kolis, J. W. Hydrothermal Synthesis as a Route to Mineralogically-Inspired Structures. *Dalton Trans.* **2016**, *45*, 2772−2784.

(5) Ötvös, S. B.; Mészáros, R.; Varga, G.; Kocsis, M.; Kónya, Z.; Kukovecz, Á.; Pusztai, P.; Sipos, P.; Pálinkó, I.; Fülöp, F. A Mineralogically-Inspired Silver-Bismuth Hybrid Material: An Efficient Heterogeneous Catalyst for the Direct Synthesis of Nitriles from Terminal Alkynes. *Green Chem.* **2018**, *20*, 1007−1019.



https://dx.doi.org/10.1021/acs.inorgchem.9b02565
*Inorg. Chem.* XXXX, XXX, XXX−XXX

(6) Ertl, M.; Andronescu, C.; Moir, J.; Zobel, M.; Wagner, F. E.; Barwe, S.; Ozin, G.; Schuhmann, W.; Breu, J. Oxygen Evolution Catalysis with Mössbauerite - A Trivalent Iron-Only Layered Double Hydroxide. *Chem. - Eur. J.* **2018**, *24*, 9004−9008.
(7) Vergasova, L. P.; Filatov, S. K. A Study of Volcanogenic Exhalation Mineralization. *J. Volcanol. Seismol.* **2016**, *10*, 71−85.
(8) Krivovichev, S. V.; Mentré, O.; Siidra, O. I.; Colmont, M.; Filatov, S. K. Anion-Centered Tetrahedra in Inorganic Compounds. *Chem. Rev.* **2013**, *113*, 6459−6535.
(9) Fujihala, M.; Koorikawa, H.; Mitsuda, S.; Morita, K.; Tohyama, T.; Tomiyasu, K.; Koda, A.; Okabe, H.; Itoh, S.; Yokoo, T.; Ibuka, S.; Tadokoro, M.; Itoh, M.; Sagayama, H.; Kumai, R.; Murakami, Y. Possible Tomonaga-Luttinger Spin Liquid State in the Spin-1/2 Inequilateral Diamond-Chain Compound $K_3Cu_3AlO_2(SO_4)_4$. *Sci. Rep.* **2017**, *7*, 16785.
(10) Volkova, L. M.; Marinin, D. V. Frustrated Antiferromagnetic Spin Chains of Edge-Sharing Tetrahedra in Volcanic Minerals $K_3Cu_3(Fe_{0.82}Al_{0.18})O_2(SO_4)_4$ and $K_4Cu_4O_2(SO_4)_4$MeCl. *J. Supercond. Novel Magn.* **2017**, *30*, 959−971.
(11) Badrtdinov, D. I.; Kuznetsova, E. S.; Verchenko, V. Yu.; Berdonosov, P. S.; Dolgikh, V. A.; Mazurenko, V. V.; Tsirlin, A. A. Magnetism of Coupled Spin Tetrahedra in Ilinskite-Type $KCu_5O_2(SeO_3)_2Cl_3$. *Sci. Rep.* **2018**, *8*, 2379.
(12) Vergasova, L. P.; Starova, G. L.; Filatov, S. K.; Anańev, V. V. Averievite $Cu_5(VO_4)_2O_2{\cdot}$nMX - a New Mineral of Volcanic Exhalations. *Dokl. Akad. Nauk* **1998**, *359*, 804−807.
(13) Botana, A. S.; Zheng, H.; Lapidus, S. H.; Mitchell, J. F.; Norman, M. R. Averievite: a Copper Oxide Kagome Antiferromagnet. *Phys. Rev. B: Condens. Matter Mater. Phys.* **2018**, *B98*, 054421.
(14) Queen, W. L.; West, J. P.; Hwu, S. J.; VanDerveer, D. G.; Zarzyczny, M. C.; Pavlick, R. A. The versatile chemistry and noncentrosymmetric crystal structures of salt-inclusion vanadate hybrids. *Angew. Chem., Int. Ed.* **2008**, *47*, 3791−3794.
(15) Martin, F. D.; Mueller Buschbaum, H. Zur Kenntnis von $K_4CuV_5O_{15}Cl$. *Z. Naturforsch., B: J. Chem. Sci.* **1994**, *B49*, 1459−1462.
(16) Martin, F. D.; Mueller Buschbaum, H. Synthese und Kristallstruktur eines Alkali-Erdalkali-Kupfer-Halogeno-Oxovanadats: $KBaCuV_2O_7Cl$. *Z. Naturforsch., B: J. Chem. Sci.* **1994**, *B49*, 355−359.
(17) Sun, K.; Litvinchuk, A. P.; Tapp, J.; Moeller, A. Synthesis, crystal structures, magnetic properties, and lattice dynamics of $Ba_2XCu(OH)[V_2O_7]$ with X = Cl, Br. *J. Solid State Chem.* **2016**, *236*, 69−77.
(18) Pekov, I. V.; Zubkova, N. V.; Zelenski, M. E.; Yapaskurt, V. O.; Polekhovsky, Yu.S.; Fadeeva, O. A.; Pushcharovsky, D. Yu. Yaroshevskite, $Cu_9O_2(VO_4)_4Cl_2$, a New Mineral from the Tolbachik Volcano, Kamchatka, Russia. *Mineral. Mag.* **2013**, *77*, 107−116.
(19) Kovrugin, V. M.; Siidra, O. I.; Colmont, M.; Mentré, O.; Krivovichev, S. V. Emulating Exhalative Chemistry: Synthesis and Structural Characterization of Ilinskite, $Na[Cu_5O_2](SeO_3)_2Cl_3$, and Its K-Analogue. *Mineral. Petrol.* **2015**, *109*, 421−430.
(20) Kovrugin, V. M.; Colmont, M.; Siidra, O. I.; Mentré, O.; Al-Shuray, A.; Gurzhiy, V. V.; Krivovichev, S. V. Oxocentered Cu(II) Lead Selenite Honeycomb Lattices Hosting $Cu(I)Cl_2$ Groups Obtained by Chemical Vapor Transport Reactions. *Chem. Commun.* **2015**, *51*, 9563−9566.
(21) Kovrugin, V. M.; Colmont, M.; Siidra, O. I.; Gurzhiy, V. V.; Krivovichev, S. V.; Mentré, O. Pathways for Synthesis of New Selenium-Containing Oxo-Compounds: Chemical Vapor Transport Reactions, Hydrothermal Techniques and Evaporation Method. *J. Cryst. Growth* **2017**, *457*, 307−313.
(22) Kovrugin, V. M.; Nekrasova, D. O.; Siidra, O. I.; Mentré, O.; Masquelier, C.; Stefanovich, S. Yu; Colmont, M. Mineral-Inspired Crystal Growth and Physical Properties of $Na_2Cu(SO_4)_2$, and Review of $Na_2M(SO_4)_2(H_2O)_x$ (x = 0−6) Compounds. *Cryst. Growth Des.* **2019**, *19*, 1233−1244.
(23) Mercurio-Lavaud, D.; Frit, B. Structure Cristalline de la Variete Haute Temperature du Pyrovanadate de Cuivre: $Cu_2V_2O_7$ beta. *CR Acad. Sci. C Chim.* **1973**, *277*, 1101−1104.
(24) Cudennec, Y.; Riou, A.; Gerault, Y.; Lecerf, A. Synthesis and Crystal Structures of Cd(OH)Cl and Cu(OH)Cl and Relationship to Brucite Type. *J. Solid State Chem.* **2000**, *151*, 308−312.
(25) Sheldrick, G. M. Crystal Structure Refinement with SHELXL. *Acta Crystallogr., Sect. C: Struct. Chem.* **2015**, *C71*, 3−8.
(26) Petříček, V.; Dušek, M.; Palatinus, L. Crystallographic Computing System JANA2006: General Features. *Z. Kristallogr. - Cryst. Mater.* **2014**, *229*, 345−352.
(27) Chukanov, N. V.; Chervonnyi, A. D. *Infrared Spectroscopy of Minerals and Related Compounds* **2016**, 1109.
(28) Koepernik, K.; Eschrig, H. Full-potential nonorthogonal local-orbital minimum-basis band-structure scheme. *Phys. Rev. B: Condens. Matter Mater. Phys.* **1999**, *59*, 1743−1757.
(29) Perdew, J. P.; Burke, K.; Ernzerhof, M. Generalized gradient approximation made simple. *Phys. Rev. Lett.* **1996**, *77*, 3865−3868.
(30) Xiang, H. J.; Kan, E. J.; Wei, S.-H.; Whangbo, M.-H.; Gong, X. G. Predicting the spin-lattice order of frustrated systems from first principles. *Phys. Rev. B: Condens. Matter Mater. Phys.* **2011**, *84*, 224429.
(31) Islam, S. S.; Ranjith, K. M.; Baenitz, M.; Skourski, Y.; Tsirlin, A. A.; Nath, R. Frustration of square cupola in $Sr(TiO)Cu_4(PO_4)_4$. *Phys. Rev. B: Condens. Matter Mater. Phys.* **2018**, *97*, 174432.
(32) Colmont, M.; Darie, C.; Tsirlin, A. A.; Jesche, A.; Colin, C.; Mentré, O. Compressibility of $BiCu_2PO_6$: Polymorphism against $S$ = 1/2 magnetic spin ladders. *Inorg. Chem.* **2018**, *57*, 6038−6044.
(33) Jahn, H. A.; Teller, E. Stability of Polyatomic Molecules in Degenerate Electronic States. *Proc. R. Soc. London* **1937**, *A161*, 220−235.
(34) Liebau, F. Structural chemistry of silicates. *Structure, Bonding and Classification*; Springer Verlag: Berlin, 1985.
(35) Siidra, O. I.; Kozin, M. S.; Depmeier, W.; Kayukov, R. A.; Kovrugin, V. M. Copper-Lead Selenite Bromides: A New Large Family of Compounds Partly Having $Cu^{2+}$ Substructures Derivable from Kagome-nets. *Acta Crystallogr., Sect. B: Struct. Sci., Cryst. Eng. Mater.* **2018**, *B74*, 712−724.
(36) Mekata, M. Kagome: The Story of the Basketweave Lattice. *Phys. Today* **2003**, *56*, 12−13.
(37) Pregelj, M.; Zaharko, O.; Günther, A.; Loidl, A.; Tsurkan, V.; Guerrero, S. Magnetic Ground State and Two-Dimensional Behavior in Pseudo-Kagome Layered System $Cu_3Bi(SeO_3)_2O_2Br$. *Phys. Rev. B: Condens. Matter Mater. Phys.* **2012**, *B86*, 144409.
(38) Constable, E.; Raymond, S.; Petit, S.; Ressouche, E.; Bourdarot, F.; Debray, J.; Josse, M.; Fabelo, O.; Berger, H.; de Brion, S.; Simonet, V. Magnetic and Dielectric Order in the Kagomelike Francisite $Cu_3Bi(SeO_3)_2O_2Cl$. *Phys. Rev. B: Condens. Matter Mater. Phys.* **2017**, *B96*, 014413.
(39) Rousochatzakis, I.; Richter, J.; Zinke, R.; Tsirlin, A. A. Frustration and Dzyaloshinsky-Moriya Anisotropy in the Kagome Francisites $Cu_3Bi(SeO_3)_2O_2X$ ($X$=Br, Cl). *Phys. Rev. B: Condens. Matter Mater. Phys.* **2015**, *B91*, 024416.


https://dx.doi.org/10.1021/acs.inorgchem.9b02565
*Inorg. Chem.* XXXX, XXX, XXX−XXX